Article

Synthesis of Active Platinum#Silver Alloy Electrocatalyst toward the Formic Acid Oxidation Reaction

J. B. Xu, T. S. Zhao, and Z. X. Liang

J. Phys. Chem. C, **2008**, 112 (44), 17362-17367 • DOI: 10.1021/jp8063933 • Publication Date (Web): 15 October 2008

Synthesis of Active Platinum−Silver Alloy Electrocatalyst toward the Formic Acid Oxidation Reaction

J. B. Xu, T. S. Zhao,* and Z. X. Liang

Department of Mechanical Engineering, The Hong Kong University of Science and Technology, Clear Water Bay, Kowloon, Hong Kong SAR, China

Received: July 20, 2008; Revised Manuscript Received: August 23, 2008

Bimetallic Pt−Ag alloy nanoparticles supported on carbon powder were successfully prepared by the coreduction method using *N*,*N*-dimethylformamide as a three-functional solvent, ligand, and reductant in an alkaline medium at room temperature. X-ray diffraction analyses confirmed the formation of face-centered cubic crystal Pt−Ag alloy nanoparticles on the carbon powder. Transmission electron microscopy and energy-dispersive X-ray spectrometer results indicated that well-dispersed Pt−Ag particles (2−4 nm) with the controlled composition (1:1) were formed on the carbon support. X-ray photoelectron spectroscopy measurements revealed that 77% of Pt is present in its metallic state. The alloy-dependent catalytic properties of the PtAg/C alloy nanoparticles were analyzed by cyclic voltammetry method through the formic acid electrooxidation reaction. As compared with the commercial carbon-supported Pt, the PtAg/C synthesized by the method developed in this work gave a lower onset potential, lower peak potential, and higher peak current for the formic acid oxidation reaction.

Introduction

Owing to their small sizes and extremely large surface areas, nanosized metal particles are known to have unique features, such as surface plasmon absorption, improved magnetic property, high reactivity, and enhanced catalytic activity.[1−4] These features may be enhanced, modified, or suppressed in case nanoparticles are formed with bimetals and multimetals. These possible changes in material properties are due to the intermetallic interactions that arise from their constitutional and morphological combinations.[5−7] The electrocatalysts for low-temperature fuel cells are typically composed of bimetallic platinum-based nanoparticles. The modifications in the structural and electronic properties of active catalytic sites that result from the use of those bimetallic catalysts make it possible to dramatically improve the activity, selectivity, and durability of the catalysts.[8] The electrooxidation of formic acid on bimetallic platinum-based nanoparticles has been extensively studied not only as a model reaction in electrocatalysis but also as a candidate for the anodic reaction in low-temperature fuel cells. A significant increase in the rate of the formic acid oxidation was found on Pt−Ru, Pt−Bi, and Pt−Au surfaces on the basis of a bifunctional mechanism, an electronic effect, or an ensemble effect.[9] The theoretical analysis indicated that Pt−Ag alloy nanoparticles might be a promising anode catalyst for the formic acid oxidation reaction with the mechanism similar to that of Pt−Au based on the ensemble effect.[10] However, few studies have been reported on the catalytic behavior of the Pt−Ag alloy nanoparticles, especially for the electrooxidation of formic acid. In this work, we intended to gain an understanding of the influence of Ag on Pt−Ag alloy in the electrooxidation of formic acid.

The catalytic properties of the metal alloy nanoparticles are closely dependent on the method of preparation. Alloy nanoparticles can be conveniently synthesized by simultaneous reduction of two or more metal ions.[11,12] However, the synthesis of single-phase Pt−Ag alloy nanoparticles is complicated because of the different reduction kinetics of Pt and Ag ions[11] and the thermodynamic immiscibility.[13] For instance, as reported by many investigators, phase segregations were observed in preparation of Pt−Ag bimetallic nanoparticles via coreduction method.[11,14,15] Although the successful preparation of Pt−Ag alloy colloids and Pt−Ag alloy nanoparticles has been reported, the composition control in single particles is still hard to achieve.[16,17] Hence, the synthesis of Pt−Ag alloy nanoparticles is a complex problem because of the composition control in addition to size and size distribution control. From the point view of composition control, the molecular precursor approach has several intrinsic advantages, namely, assurance of molecular level mixing between the constituent metals and a predetermined stoichiometry based on the atomic composition in the precursor.[18] Despite these apparent advantages, reports on the single-source precursor synthesis of Pt−Ag alloy nanoparticles remain scarce because most of the single-source precursors are air- and moisture-sensitive so that their preparation and handling warrant special precaution. Another concern with the bimetallic cluster precursor approach, however, is whether the different metals will segregate either immediately upon contact with the support or under the conditions necessary to form an active catalyst. Recently, we found that Pt−Au alloy nanoparticles with a controlled composition in single particles can be obtained using *N*,*N*-dimethylformamide (DMF)-coordinated Pt−Au complex as a precursor.[19] This approach offers the potential of controlling the composition of the derived catalyst particles, allowing one to probe the role of the individual components in a bimetallic catalyst. In this work, we prepared the DMF-coordinated Pt−Ag complex and used it as the precursor for the synthesis of Pt−Ag alloy nannoparticles.

In practical applications, finely dispersed metal nanoparticles supported on inorganic carriers are a mainstay of commercial heterogeneous catalysts and are employed in numerous industrial reactions and fuel cell technologies.[20−22] In this work, we used

* Corresponding author. Tel.: (852) 2358 8647. E-mail: metzhao@ust.hk.

10.1021/jp8063933 CCC: $40.75
Published on Web 10/15/2008

carbon powder as a support for the synthesis of Pt−Ag alloy catalyst. The prepared nanoparticles were characterized with X-ray diffraction (XRD), transmission electron microscopy (TEM), energy-dispersive X-ray spectrometer (EDS), and X-ray photoelectron spectroscopy (XPS). The alloy-dependent catalytic properties of the Pt−Ag nanoparticles were characterized by cyclic voltammetry (CV) method through the formic acid electrooxidation reaction.

Experimental Section

Materials. All of the chemicals used were of analytical grade. Hexachloroplatinic acid and silver nitrate were purchased from Aldrich. DMF, ethanol, formic acid, perchloric acid, sodium hydroxide, and potassium chloride (all from Merck KGaA) were used as received. Vulcan XC-72 carbon (particle size 20−40 nm) and carbon-supported Pt catalyst (20 wt %) were procured from E-TEK Company. Nafion solution (5 wt %) was received from Dupont and used as received.

Characterization Methods. UV−vis absorption spectra were measured on a Milton Roy Spectronic 3000 Array spectrophotometer. The XRD patterns of the Pt/C and PtAg/C nanocatalysts were obtained with a Philips powder diffraction system (model PW 1830) using a Cu Kα source operating at 40 keV at a scan rate of 0.025° s^{-1}. TEM images were obtained by using a high-resolution JEOL 2010F TEM system operating with a LaB6 filament at 200 kV. The samples were dispersed in ethanol under sonication and dropped on the carbon-coated grid and then imaged. The atomic compositions of the Pt−Ag nanoparticles supported on Vulcan XC-72 carbon were analyzed by EDS, which was integrated with the TEM instrument. The surface characterization was carried out by the XPS technique, which is equipped with a Physical Electronics PHI 5600 multitechnique system using Al monochromatic X-ray at a power of 350 W. The survey and regional spectra were obtained by passing energy of 187.85 and 23.5 eV, respectively.

Preparation of the Carbon-Supported Pt−Ag Alloy Nanoparticles. The DMF-coordinated Pt−Ag complex precursor was prepared as follows: 10 mL of 10 mM H_2PtCl_6 and $AgNO_3$ DMF solution was mixed and illuminated with UV light (250 nm, 300 W) for 3 h.[19] A gradual color change was observed concomitantly with the dissolution of AgCl, and a nearly colorless solution was obtained in 3 h. Carbon powder (121 mg) was suspended in the resulting solution under vigorous stirring. After a homogeneous suspension was formed, 20 mL of 0.2 M NaOH solution was added to the mixture under steady stirring at room temperature. After being stirred for 40 min, the precipitate thus formed was collected by centrifugation, washed several times with ethanol and water, and dried at 70 °C in oven (Pt−Ag loading: 20 wt %, with platinum-to-silver mole ratio of 1).

Preparation of the Working Electrode. Glassy carbon electrode (GCE) (Taizhou Electroanalytical Instrument Factory, 4 mm in diameter) was polished to a mirror finish with 0.05-μm alumina suspension before each experiment and served as an underlying substrate of the working electrode. The catalyst ink was prepared by ultrasonically dispersing 10 mg of 20 wt % of Pt/C and PtAg/C in 1.9 mL of ethanol, to which 0.1 mL of 5 wt % Nafion solution was added, and the dispersion was ultrasonicated for 30 min to obtain a homogeneous solution. A quantity of 9 μL of the dispersion was pipetted out on top of the GCE and dried in air to yield a metal loading of 72 μg cm^{-2}.

Electrochemical Measurements. Electrochemical measurements were carried out by CV using a potentiostat (EG&G Princeton, model 273A). A conventional, three-electrode cell consisting of GCE with an area of 0.125 cm^2 as the working electrode, Pt foil as the counter electrode, and a saturated calomel electrode as the reference electrode was used. The reference electrode was placed in a separate chamber, which was located near the working electrode through a Luggin capillary tube. The CV experiments were performed in 0.5 M $HClO_4$ solution containing 0.25 M HCOOH at a scan rate of 50 mV s^{-1}. Solutions were prepared from analytical grade reagents and DI water. All experiments were done at room temperature in nitrogen (99.9%)-saturated solutions. In all of the experiments, stable voltammogram curves were recorded after scanning for 20 cycles in the potential region from −0.2 to 0.8 V in 0.5 M $HClO_4$ solution.

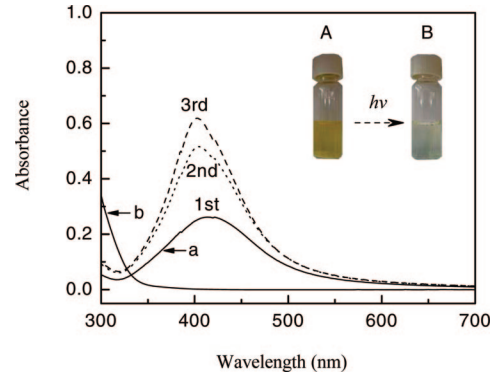

Figure 1. Absorption spectra of Ag−DMF (a) and Pt−Ag−DMF (b). Inset is the digital camera image of mixed $AgNO_3/H_2PtCl_6$ and Pt−Ag complex in DMF.

Results and Discussion

Characterization of the Pt−Ag Complex Precursor. The presence of Pt−Ag interaction in solution was characterized by UV−vis measurements. Figure 1 compares the UV−vis spectra of $AgNO_3$ (curve a) and Pt−Ag complex (curve b) in DMF at a concentration of 0.8 mM. Note that the images of both mixed $AgNO_3/H_2PtCl_6$ and Pt−Ag complex in DMF are also shown in Figure 1. It is seen from Figure 1 that the absorbance maximum of curve a appeared at ∼416 nm, and the peak absorbance became sharper and increased in intensity at continuous tests. This broad absorbance peak potentially results from the formed spherical silver nanoparticles.[23] It was reported that the spontaneous reduction of Ag^+ ions in DMF can be performed at room temperature even in the dark and the use of visible or UV radiation will accelerate this process.[24] However, the silver surface plasmon absorption peak was quenched in Pt−Ag complex during the UV measurement (curve b). This observation suggests that the presence of Pt^{4+} ions prevents the Ag^+ ions from reducing in DMF, which indicates the Pt−Ag interaction formation in DMF solution. This result is consistent with the Pt−Au complex reported elsewhere.[19] This Pt−Ag interaction in solution offers the possible nucleation of Pt−Ag alloy particles with the atomic-level mixing at coreduction. In this work, we prepared the carbon-supported $Pt_{50}Ag_{50}$ nanoparticles and investigated their morphological, compositional, structural, and catalytic properties.

Physicochemical Characterization of the Carbon-Supported Pt−Ag Alloy Nanoparticles. To get the information on the average particle size and the Pt−Ag alloy effect, the PtAg/C sample was characterized by XRD, and the result is shown in Figure 2, along with the diffraction pattern of the Pt/C catalyst as a comparison. The pattern of the PtAg/C exhibited

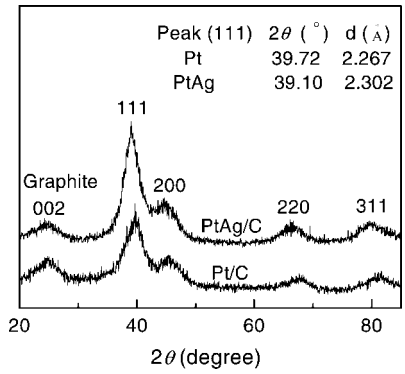

Figure 2. XRD pattern of bimetallic PtAg/C and Pt/C samples.

diffraction peaks of (111), (200), (220), and (311) at 2θ values of 39.1°, 44.9°, 66.4°, and 79.9°, respectively. These peaks indicate that Pt is present in the face-centered cubic structure.[25] Compared to that of the Pt/C, the shift of the (111) peak to a lower 2θ angle by about 0.6° could be indexed to a higher d space (d_{111} = 2.302 Å) crystal structure of Pt because of incorporation of the Ag atoms, indicating that the single-phase Pt−Ag alloy was formed on the carbon powder.[26] The average particle size of PtAg/C catalysts was 2.4 nm, as calculated from the broadening of the (220) diffraction peaks using Scherrer's equation[27]

$$d = \frac{0.9\lambda}{B_{2\theta} \cos \theta_{\max}} \quad (1)$$

where λ is the wavelength of the X-ray (1.54056 Å), θ is the angle at the maximum of the peak, and $B_{2\theta}$ is the width of the peak at half-height.

Figure 3 shows the typical TEM images of the PtAg/C sample at different scales. It can be observed from Figure 3a that Pt−Ag alloy nanoparticles, roughly in the spherical shape, are well-dispersed without aggregations. The evaluation of the characteristic diameter of the Pt−Ag particles from an ensemble of 150 particles in an arbitrarily chosen area of the high-resolution TEM (HRTEM) images results in a narrow size distribution from 2.0 to 4.3 nm with an average diameter of 2.9 nm, which is consistent with the calculated value by XRD, as discussed earlier. From the HRTEM image shown in Figure 3b, it can be seen that the Pt−Ag nanoparticles appear to be entirely crystalline, as evidenced by the lattice fringes across the full extent of the image. The composition of a single Pt−Ag particle (randomly chosen) was analyzed by EDS, and the result is shown in Figure 4, which indicates an elemental composition of 50.4% Pt and 49.6% Ag in the alloy. This result is consistent with the Pt:Ag ratio in the precursor (with silver-to-platinum mole ratio of 1).

XPS was employed to analyze the valence state and the surface composition of the carbon-supported metals. Figure 5 shows the regional Pt4f spectra of the PtAg/C and Pt/C samples. The Pt4f spectra show a doublet containing a low energy band ($Pt4f_{7/2}$) and a high energy band ($Pt4f_{5/2}$) at 70.9 and 74.2 eV for PtAg/C and 71.5 and 74.8 eV for Pt/C, respectively, indicating the existence of metallic state Pt.[28] However, the clear shifts of the peak positions can be observed for Pt4f, and the decrease in the Pt binding energies for PtAg/C relative to that of Pt/C suggests electron transfer from Ag to Pt, which can be related to the perturbed electronic interaction between Pt and Ag atomic orbit and in turn to its alloy formation.[29] To identify different chemical states of Pt, the spectrum can be fitted by three pairs of overlapping Lorentzian curves. Figure 6a shows the Pt4f spectrum of Pt/C, which was deconvoluted into three components, as labeled by 1, 2, and 3 with respective binding energies of 71.5, 72.8, and 75.5 eV. These three pairs of peaks indicated that Pt is present in three different oxidation states. The most intense peaks with $Pt4f_{7/2}$ signal at 71.5 eV were due to metallic Pt. The second set of doublets, observed at binding energy 1.3 eV higher than that of Pt(0), could be attributed to the Pt(II) chemical state on PtO or $Pt(OH)_2$. The third pair of curves corresponded to the Pt(IV) species.[30] The amount of Pt species was calculated from the relative intensities of these three peaks, and the results are summarized in Table 1. Here again, the Pt4f spectrum of PtAg/C could be deconvoluted into three components, as labeled by 1, 2, and 3 in Figure 6b. The binding energies of the Pt $4f_{7/2}$ signal for the different components in the samples are given in Table 1. Akin to the XPS spectrum of the Pt/C sample, the components 1, 2, and 3 are ascribed to Pt(0), Pt(II), and Pt(IV) signals, respectively; the respective relative intensities of these components are 77, 16, and 7 (Table 1). The XPS result indicates that metallic Pt(0) is the predominant species. The relatively higher amount of Pt(0) species present in the PtAg/C sample can be explained on the basis of electron transfer from Ag to Pt.[29] Furthermore, on the basis of the intensities of the XPS peaks, the elemental composition of the bimetallic nanoparticles could be obtained with the surface atomic ratio of Pt−Ag is 1:1, which agrees well with the EDS analysis.

Electrochemical Characterization of the Pt−Ag Alloy Nanoparticles. Figure 7 compares the typical CV curves of the PtAg/C and Pt/C catalysts measured in the potential range between −0.2 and 1.2 V in 0.5 M $HClO_4$ at a sweep rate of 50 mV s^{-1}. For the first cycle of the PtAg/C alloy electrode (the red line), an obvious anodic peak was observed at ∼0.86 V due to the formation of oxide species for Pt and Ag. However, after several cycles, this peak disappeared and a steady-state electrode surface was obtained at last. The nature of these changes is that the base voltammetry becomes more "Pt-like", probably indicative of leaching of Ag from the surface. As can be seen in Figure 7, the voltammetric features of the stabilized PtAg/C electrode (the solid line) are very similar to those of a polycrystalline Pt electrode (the dash line): the adsorption and desorption of hydrogen within the potential range of −0.20 to 0.08 V, the double-layer capacitance region between 0.08 and 0.56 V, the formation of Pt oxides at potentials more positive than 0.56 V, and the reduction of Pt oxides in the cathodic potential scan.[31] Such voltammetric features have been observed with other Pt-based alloys such as PtFe, PtNi, and PtCo, and they are ascribed to the formation of a "Pt skin" on the catalyst surface.[25,32,33]

To understand the electrocatalytic behavior of the Pt−Ag alloy and the "Pt skin" catalysts, the different cycles of the CV test toward the formic acid oxidation reaction were recorded. Figure 8 shows CV curves of the Pt−Ag alloy (the first cycle) and the "Pt skin" (the 40th cycle) of the PtAg/C catalyst, together with the Pt/C catalyst on the same scale. It can be seen that the formic acid electrooxidation on the Pt/C electrode (the dash line) shows two anodic peaks in the forward scan. The first small anodic peak (∼0.30 V) is attributed to the direct oxidation of formic acid to CO_2 on the remaining sites unblocked by intermediary species. The second peak and gradual increase of anodic current up to about 0.66 V on the anodic scan are related to the oxidation of adsorbed intermediary species (CO), which releases the free surface sites for the subsequent direct oxidation of formic acid. In the backward scan, it is the bulk HCOOH oxidation peak, which occurs at approximately

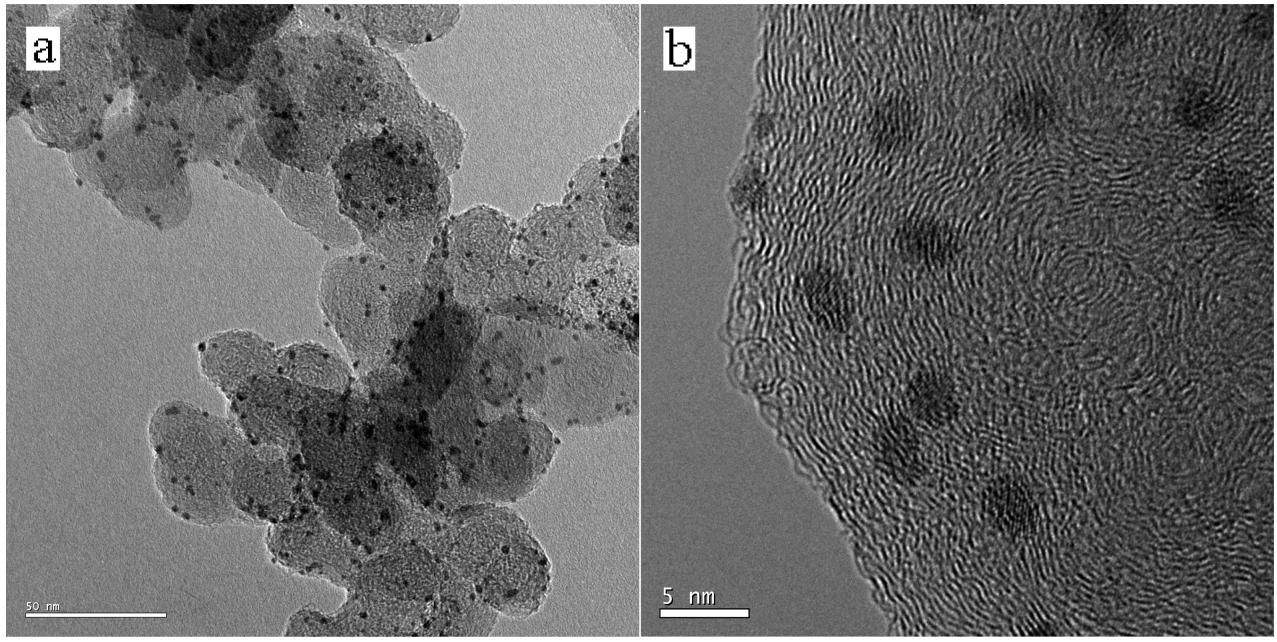

Figure 3. TEM (a) and HRTEM (b) images of PtAg/C.

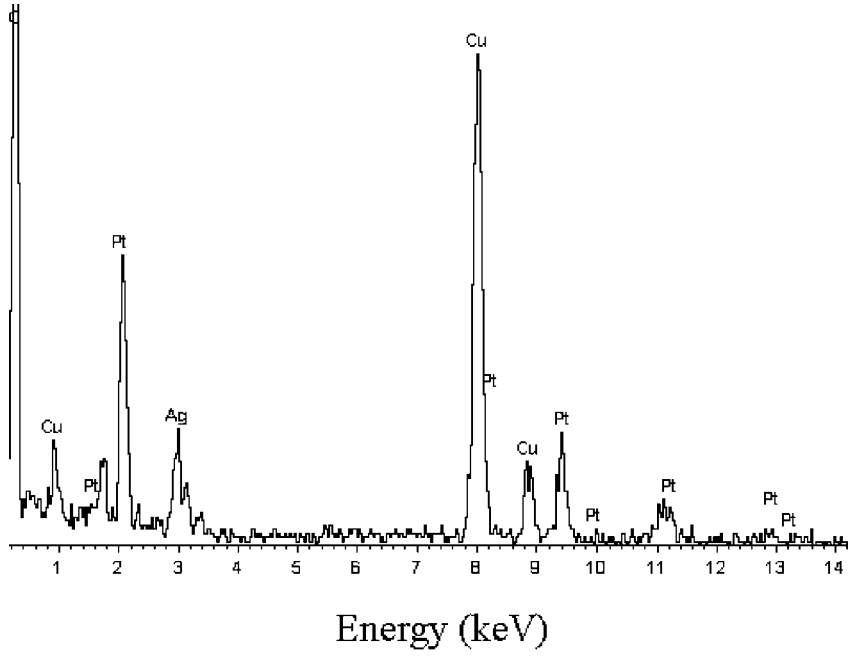

Figure 4. EDS spectrum of a single Pt−Ag alloy particle.

the same potential as the first anodic peak.[34] The same situation was observed for the "Pt skin" electrode (the solid line). In comparison, the Pt−Ag alloy electrode (the red line) exhibited significantly enhanced catalytic activity for formic acid oxidation relative to the unalloyed Pt as well as "Pt skin" electrodes, particularly in the low potential region. It can been seen from Figure 8 that the first anodic peak occurred at ∼0.25 V. This negative shift of the peak potential indicates the higher catalytic activity of the Pt−Ag alloy catalyst toward formic acid electrooxidation as compared with that of the Pt/C catalyst. This higher catalytic activity may be due to the high percentage of the Pt^0 species due to the electron transfer from Ag to Pt.[29] As for the second peak, it shows a positive shift to ∼0.90 V. This result indicates that the Pt−Ag alloy catalyst shows lower catalytic activity for CO species as compared with the Pt/C

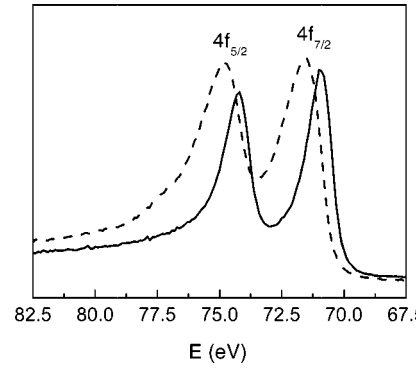

Figure 5. Pt4f XPS spectra of the Pt/C (dashed line) and PtAg/C (solid line).

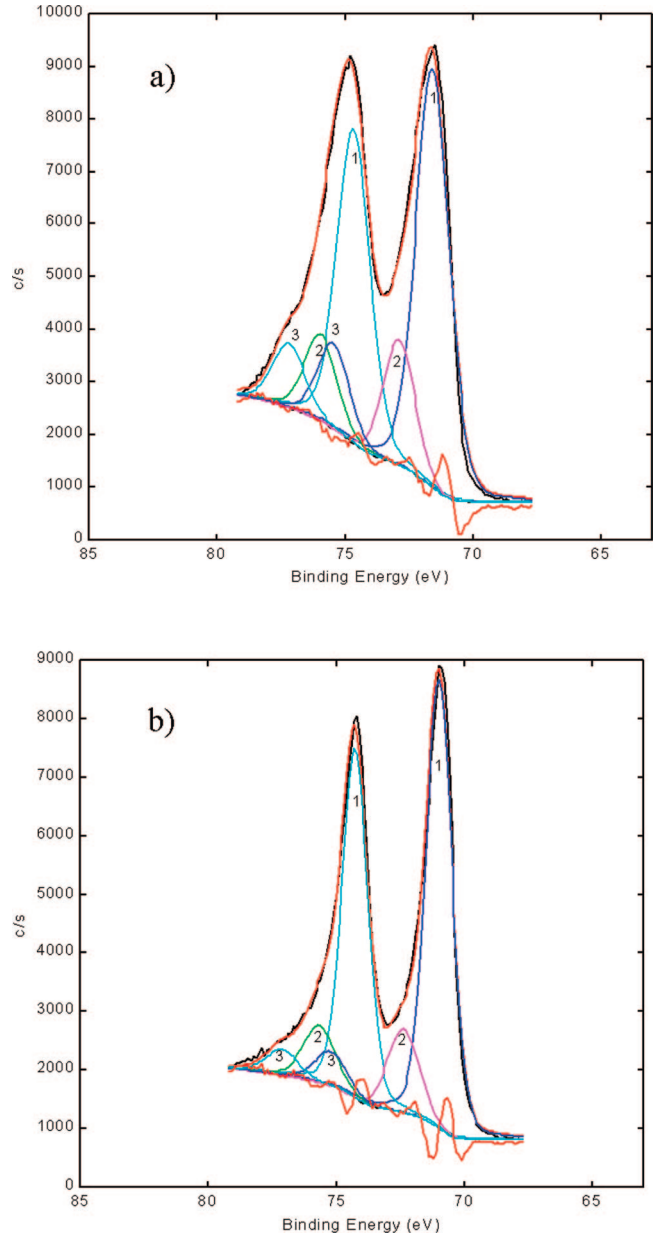

Figure 6. Pt4f XPS spectra of the Pt/C (a) and PtAg/C (b) fitted by three pairs of overlapping Lorentzian curves labeled by 1, 2, and 3.

TABLE 1: Binding Energies and Relative Intensities of Different Platinum Species of Pt/C and PtAg/C Samples

sample	species	binding energy ($4f_{7/2}$)	relative intensity (%)
Pt/C	Pt(0)	71.5	69
	Pt(II)	72.8	18
	Pt(IV)	75.5	13
PtAg/C	Pt(0)	71.0	77
	Pt(II)	72.4	16
	Pt(IV)	75.2	7

catalyst. This result is consistent with Hwang et al.'s work.[26] It has been demonstrated that the alloying of Ag with Pt makes the oxidation of CO on the Pt surface sluggish because of the electronic effect. By comparing the intensity of these two anodic peaks, it can be observed that the formic acid oxidation on the PtAg/C alloy catalyst shifts toward the dehydrogenation branch in contrast with the Pt/C catalyst.[34] This behavior can be explained by the ensemble effect. It was reported that the noncontinuous Pt sites favor the dehydrogenation process in the presence of the neighboring Pt and Ag sites, which confirms

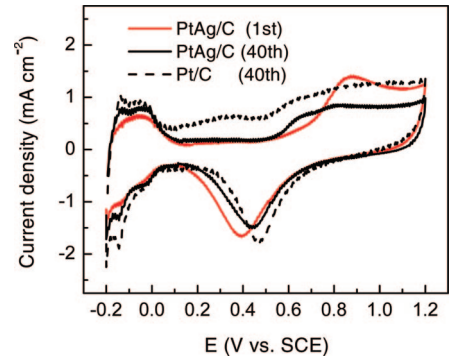

Figure 7. CV curves of the PtAg/C and Pt/C catalysts in 0.5 M $HClO_4$ at the sweep rate of 50 mV s^{-1}.

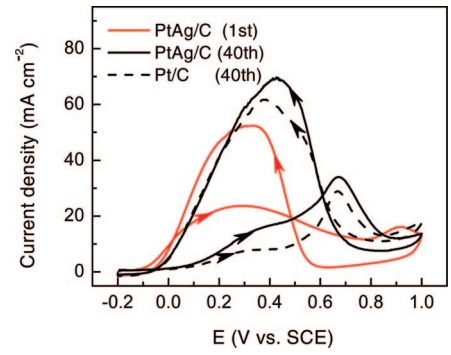

Figure 8. CV curves of the PtAg/C and Pt/C catalysts in 0.5 M $HClO_4$ containing 0.25 M HCOOH at the sweep rate of 50 mV s^{-1}.

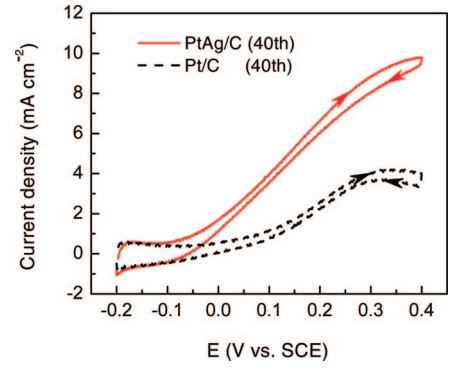

Figure 9. CV curves of the PtAg/C and Pt/C catalysts in 0.5 M $HClO_4$ containing 0.25 M HCOOH at the sweep rate of 50 mV s^{-1}.

the atomic-level mixing Pt−Ag alloy nanoparticles formation with this method.[19,34,35]

To investigate the catalytic activity before silver dissolution and CO_{ads} species oxidation, the CV test in the potential range between −0.2 and 0.4 V was recorded. It can be seen in Figure 9 that the Pt−Ag alloy catalyst shows the higher electrocatalytic activity in terms of its lower onset potential and higher peak current than those of the Pt/C catalyst. This high catalytic activity in the low potential region suggests that the PtAg/C is a promising anode catalyst for direct formic acid fuel cells.

Conclusions

In this work, the uniform Pt−Ag alloy nanoparticles supported on carbon powder were successfully prepared by the coreduction method in DMF. The XRD analysis confirmed the formation of single-phase Pt−Ag alloy nanoparticles on the carbon powder. The TEM and EDS results indicated that well-dispersed Pt−Ag particles (2−4 nm in size) with the controlled composition (1:1) were formed on the carbon support. The XPS

measurements revealed that the amount of Pt presented in its metallic states in the PtAg/C is 77%, which is higher than that in the Pt/C (69%), because of the electron transfer from Ag to Pt. The alloy-dependent catalytic properties of the PtAg/C alloy nanoparticles were analyzed by CV method through formic acid electrooxidation reaction. The result demonstrated that the PtAg/C synthesized by this method exhibited higher catalytic activity than did the commercial Pt/C catalyst in terms of its lower onset potential, lower peak potential, and higher peak current for the formic acid oxidation reaction.

Acknowledgment. The work described in this article was fully supported by a grant from the Research Grants Council of the Hong Kong Special Administrative Region, China (Project No. 622807).

References and Notes

(1) Schmid, G. *Chem. Rev.* **1992**, *92*, 1709.
(2) Schmid, G.; Hornyak, G. L. *Curr. Opin. Solid State Mater. Sci.* **1997**, *2*, 204.
(3) Pileni, M. P. In *Metal Nanoparticles: Synthesis, Characterization, and Applications*; Feldheim, D. L., Foss, C. A., Jr., Eds.; Marcel Dekker: New York, 2001; pp 207−236.
(4) (a) Toshima, N. In *Nanoscale Materials*; Liz-Marzan, L. M., Kamat, P., Eds.; Kluwer: Norwell, MA, 2003; pp 79−96. (b) Toshima, N.; Yonezawa, T. *New J. Chem.* **1998**, *22*, 1179.
(5) He, J. H.; Ichinose, I.; Kunitake, T.; Nakao, A.; Shiraishi, Y.; Toshima, N. *J. Am. Chem. Soc.* **2003**, *125*, 11034.
(6) Chen, J. Y.; Wiley, B.; McLellan, J.; Xiong, Y. J.; Li, Z. Y.; Xia, Y. N. *Nano Lett.* **2005**, *5*, 2058.
(7) Rodriguez, J. A. *Prog. Surf. Sci.* **2006**, *81*, 141.
(8) (a) Prabhuram, J.; Zhao, T. S.; Tang, Z. K.; Chen, R.; Liang, Z. X. *J. Phys. Chem. B* **2006**, *110*, 5245. (b) Jiang, L. H.; Zhou, Z. H.; Li, W. Z.; Zhou, W. J.; Song, S. Q.; Li, H. Q.; Sun, G. Q.; Xin, Q. *Energy Fuels* **2004**, *18*, 866. (c) Zhang, J.; Sasaki, K.; Sutter, E.; Adzic, R. R. *Science* **2007**, *315*, 220.
(9) (a) Markovic, N. M.; Gasteiger, H. A.; Ross, P. N., Jr.; Jiang, X.; Villegas, I.; Weaver, M. J. *Electrochim. Acta* **1995**, *40*, 91. (b) Clavilier, J.; Fernandez-Vega, A.; Feliu, J. M.; Aldaz, A. *J. Electroanal. Chem.* **1989**, *258*, 89. (c) Rach, E.; Heitbaum, J. *Electrochim. Acta* **1987**, *32*, 1173.
(10) Demirci, U. B. *J. Power Sources* **2007**, *173*, 11.
(11) Liz-Marzan, L. M.; Philipse, A. P. *J. Phys. Chem.* **1995**, *99*, 15120.
(12) (a) Link, S.; Wang, Z. I.; El-Sayed, M. A. *J. Phys. Chem. B* **1999**, *103*, 3529. (b) Mallin, M. P.; Murphy, C. J. *Nano Lett.* **2002**, *2*, 1235.
(13) Peng, Z. M.; Yang, H. *J. Solid State Chem.* **2008**, *181*, 1546.
(14) Doudna, C. M.; Bertino, M. F.; Blum, F. D.; Tokuhiro, A. T.; Lahiri-Dey, D.; Chattopadhyay, S.; Terry, J. *J. Phys. Chem. B* **2003**, *107*, 2966.
(15) Lahiri, D.; Bunker, B.; Mishra, B.; Zhang, Z.; Meisel, D.; Doundna, C. M.; Bertino, M. F.; Blum, F. D.; Tokuhiro, A. T.; Chattopadhyay, S.; Shibata, T.; Terry, J. *J. Appl. Phys.* **2005**, *97*, 094304.
(16) Torigoe, K.; Nakajima, Y.; Esumi, K. *J. Phys. Chem.* **1993**, *97*, 8304.
(17) Wu, M. L.; Lai, L. B. *Colloids Surf., A* **2004**, *244*, 149.
(18) Chandler, B. D.; Schabel, A. B.; Pignolet, L. H. *J. Phys. Chem. B* **2001**, *105*, 149.
(19) Xu, J. B.; Zhao, T. S.; Liang, Z. X.; Zhu, L. D. *Chem. Mater.* **2008**, *20*, 1688.
(20) Bird, A. J. In *Catalyst Supports and Supported Catalysts: Theoretical and Applied Concepts*; Stiles, A. B., Ed.; Butterworths: Boston, 1987; pp 107−137.
(21) Satterfield, C. N. *Heterogeneous Catalysis in Industrial Practice*; McGraw-Hill: New York, 1991.
(22) Uchida, M.; Fukuoka, Y.; Sugawara, Y.; Ohara, H.; Ohta, A. *J. Electrochem. Soc.* **1998**, *145*, 3708.
(23) Pastoriza-Santos, I.; Liz-Marzan, L. M. *Langmuir* **1999**, *15*, 948.
(24) Pastoriza-Santos, I.; Serra-Rodriguez, C.; Liz-Marzan, L. M. *J. Colloid Interface Sci.* **2000**, *221*, 236.
(25) Xu, J. B.; Hua, K. F.; Sun, G. Z.; Wang, C.; Lv, X. Y.; Wang, Y. J. *Electrochem. Commun.* **2006**, *8*, 982.
(26) Hwang, B. J.; Kumar, S. M. S.; Chen, C. H.; Chang, R. W.; Liu, D. G.; Lee, J. F. *J. Phys. Chem. C* **2008**, *112*, 2370.
(27) Liang, Z. X.; Zhao, T. S. *J. Phys. Chem. C* **2007**, *111*, 8128.
(28) Davis, D. J.; Kyriakou, G.; Lambert, R. M. *J. Phys. Chem. B* **2006**, *110*, 11958.
(29) Zeng, J. H.; Yang, J.; Lee, J. Y.; Zhou, W. J. *J. Phys. Chem. B* **2006**, *110*, 24606.
(30) Liu, F.; Lee, J. Y.; Zhou, W. *J. Phys. Chem. B* **2004**, *108*, 17959.
(31) Chen, W.; Kim, J.; Sun, S. H.; Chen, S. W. *J. Phys. Chem. C* **2008**, *112*, 3891.
(32) Chen, W.; Kim, J.; Xu, L. P.; Sun, S.; Chen, S. W. *J. Phys. Chem. C* **2007**, *111*, 13452.
(33) Stamenkovic, V.; Schmidt, T. J.; Ross, P. N.; Markovic, N. M. *J. Phys. Chem. B* **2002**, *106*, 11970.
(34) Kristian, N.; Yan, Y. S.; Wang, X. *Chem. Commun.* **2008**, 353.
(35) Park, S.; Xie, Y.; Weaver, M. J. *Langmuir* **2002**, *18*, 5792.

JP8063933